Research Article | Vol. 10, No. 10 / 1 October 2019 / Biomedical Optics Express 5130
Biomedical Optics EXPRESS

Live imaging of contracting muscles with wide-field second harmonic generation microscopy using a high power laser

HAITAO ZHAO,[1,2,3,7] RICHARD CISEK,[4,7] ABIRAMY KARUNENDIRAN,[5,6] DANIELLE TOKARZ,[4] BRYAN A. STEWART,[5,6] AND VIRGINIJUS BARZDA[2,3,*]

[1]WDI Device Inc., 135 West Beaver Creek Road Unit 2, Richmond Hill, ON, L4B 1L2, Canada
[2]Department of Chemical and Physical Sciences, University of Toronto Mississauga, 3359 Mississauga Road, Mississauga, ON L5L 1C6, Canada
[3]Department of Physics, University of Toronto, 60 St. George Street, Toronto, ON M5S 1A7, Canada
[4]Department of Chemistry, Saint Mary's University, 923 Robie Street, Halifax, NS B3H 3C3, Canada
[5]Department of Biology, University of Toronto Mississauga, 3359 Mississauga Road, Mississauga, ON L5L 1C6, Canada
[6]Department of Cell and Systems Biology, University of Toronto, 25 Harbord Street, Toronto, ON, M5S 3G5, Canada
[7]Co-first authors with equal contribution
[*]virgis.barzda@utoronto.ca

Abstract: Wide-field second harmonic generation (SHG) microscopy was developed using a high-power (> 4 W) and high-repetition-rate (MHz range) laser oscillator to achieve fast SHG imaging over a large area (400 µm × 400 µm). The microscope was used for high spatial resolution imaging of contracting muscles in live *Drosophila melanogaster* larvae. Anisotropic and isotropic bands of striated muscle were distinguished, allowing accurate determination of sarcomere length and SHG intensity from individual sarcomeres. Therefore, wide-field SHG microscopy has applications in basic contractility research and studying arrhythmias, muscular dystrophies and pharmaceutical effects on the muscle contraction dynamics of sarcomeres.

1. Introduction

Second harmonic generation (SHG) microscopy has become a technique of choice for label-free *in vivo* and *in situ* visualization of non-centrosymmetrically ordered biological structures, including collagen fibers in the extracellular matrix and myosin filaments in the sarcomeres of striated muscles [1–5]. SHG image contrast relies on the frequency-doubled response of molecules to high intensity laser pulses. For optimal SHG imaging, a laser beam from a femtosecond oscillator is focused with a microscope objective lens onto a sample, and the laser beam is raster-scanned to acquire an image either via pixel by pixel signal detection with a single element photodetector (usually a photomultiplier tube or an avalanche photodiode), or a sample is imaged onto an array detector (a charge-coupled device, CCD, or a complementary metal-oxide-semiconductor, CMOS) [6–10]. A large field of view image acquisition rate is limited by the laser scanning speed and SHG efficiency of the sample, restricting the investigations to static or slowly changing (on the order of seconds to minutes) biological structures. This ultimately poses a challenge in performing real-time imaging on a large area of the sample. On the other hand, wide-field nonlinear microscopy enables fast large area imaging however, it requires short laser pulses with high energy to achieve wide-field illumination and attain high image contrast. Amplified laser systems with µJ pulse energies and ~200 kHz pulse repetition rates have been used for wide-field SHG imaging [6,10]. Macias-Romero *et al.* revealed that indirect sample damage occurs at the pulse duration flux threshold of 12.2 mJ/cm^2 for human embryonic kidney 293 cells

#369870 https://doi.org/10.1364/BOE.10.005130
Journal © 2019 Received 18 Jun 2019; revised 29 Aug 2019; accepted 29 Aug 2019; published 13 Sep 2019

Biomedical Optics EXPRESS

at 1035 nm and 200 kHz [10]. Similarly, Harzic *et al*. reported the pulse energy threshold for Chinese hamster ovary cells as 381 mJ/cm^2 at 1035 nm and 100 kHz [11]. Therefore, pulse energy has to be kept low due to damage thresholds, the use of higher pulse repetition rates could increase SHG signal, as long as both the pulse duration flux is below threshold, and that the heat deposition due to the average laser power is kept below the physiologically relevant thermal impairment threshold. For example, König *et al.* reported that adrenal chrommafin cells had indirect damage at 5.3 mJ/cm^2 pulse energy flux, and 0.44 MW/cm^2 average power flux, at 840 nm, 190 fs and 82 MHz [12]. High pulse repetition rates in the megahertz range can be achieved by employing high power oscillators, or by amplified laser systems. In this study we utilize the simpler and more cost-effective high-power laser oscillator configuration. Furthermore, when the linear and nonlinear absorption of the sample at the laser wavelength is negligible, high laser powers can be applied to the sample without inducing adverse photo-bleaching and photo-damage effects. The imaging area can be scaled up proportionally by increasing the incident laser power while maintaining the power density below the tissue damage threshold. Optical sectioning can additionally be achieved with temporal or spectral focusing [13–16]. Therefore, wide-field SHG microscopy with high power and high pulse repetition rate lasers opens new opportunities for real-time imaging of fast structural dynamics and enables live optical biopsy and histopathology imaging on large areas.

In this paper, we used a high-power and high repetition rate laser oscillator to demonstrate the use of wide-field SHG microscopy for live imaging of contracting muscle tissue. Fast contraction dynamics over a large imaging area allowing parallel analysis of sarcomeres, to our knowledge, has not been previously demonstrated. The visualization and quantification of sarcomere contractility over a large field of view opens new possibilities for contractility research, and as a testing ground for new cardiac pharmaceutical agents.

2. Materials and methods

2.1. Wide-field SHG microscope

Wide-field SHG imaging was accomplished with a homebuilt high power ultrafast laser oscillator. The outline of the oscillator is illustrated in Fig. 1. The laser radiation is generated in a 5-atom%-doped 5-mm-long Yb:KGW crystal oriented for propagation along the Ng-axis and polarization parallel to the Np-axis [17,18]. The crystal is pumped by a fiber-coupled diode laser that provides a maximum pump power of 40 W at a central wavelength of 980 nm (Apollo Instruments, Inc.). The pump radiation is reimaged by two plano-convex lenses with focal lengths of 35 mm and 125 mm. The mode locking is self-starting and maintained by the semiconductor saturable absorber mirror (SESAM) with 1% modulation depth and 500 fs recovery time (Batop GmbH). All the highly reflective (HR) mirrors in the cavity provide -10,000 fs^2 global dispersion in a round-trip to balance the intracavity positive dispersion and the chirp induced by the self-phase-modulation. With a 7.5% output coupler, pulses with an average output power of 5.5 W at a repetition rate of 60 MHz were obtained. The central wavelength was 1041 nm and the pulse duration was measured to be ~400 fs.

Wide-field SHG imaging is accomplished with a homebuilt microscope (Fig. 1). The laser beam from the oscillator is collimated to ~4 mm in diameter and relays to an achromatic doublet with a focal length of 75 mm. In order to obtain wide-field imaging, the sample is placed above the focal plane. The image size can be adjusted by axially translating the doublet. The incident power can be tuned by rotating the half wave plate placed before a polarizing beamsplitter. The SHG signal radiated in the forward direction is collected by a microscope objective lens. Two objective lenses (Zeiss) are used in this study: a 20× 0.5 numerical aperture (NA) air objective lens and a 40× 1.3 NA oil immersion objective lens. The SHG from the sample is focused onto the electron multiplying CCD (EM-CCD, Hamamatsu ImagEM X2) by using a tube lens (f = 160 mm). The fundamental laser and fluorescence photons are filtered from SHG by a BG39 filter

Biomedical Optics EXPRESS

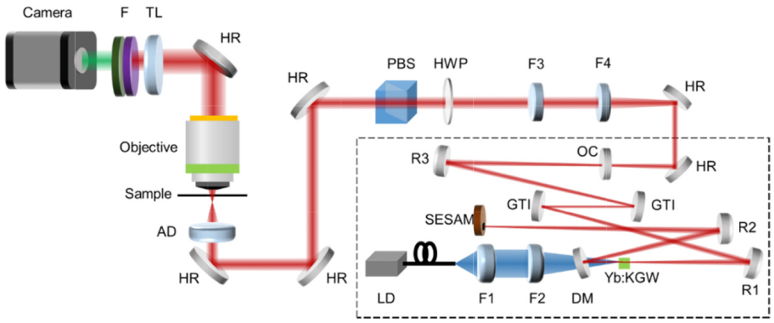

Fig. 1. Wide-field microscope with the high power oscillator (dashed rectangle). HR - highly reflective mirrors, LD - fiber-coupled diode laser, F1 ($f_1 = 35$ mm) and F2 ($f_2 = 125$ mm) - plano-convex lenses, and DM - dichroic mirror. R1, R2 and R3 - concave mirrors with radii of curvature of 350 mm, 400 mm and 600 mm, respectively, coated for high reflection at 1020-1080 nm with -1000 fs_2 group delay dispersion. OC - 7.5% output coupler. F3 ($f_3 = 200$ mm) and F4 ($f_4 = 50$ mm) - plano-convex lenses. HWP - half wave plate, PBS - polarizing beamsplitter, AD - achromatic doublet, TL - tube lens, and F – optical filters.

and a 510-520 nm band-pass interference filter (CVI Laser Optics). SHG images with 512 × 512 pixels were obtained at an acquisition rate of 10 frames per second, limited only by the number of emitted SHG photons. Faster acquisition rates could be achieved by using a lower repetition rate and higher pulse energy laser to generate more SHG signal, as long as the pulse energy fluence is below the damage threshold.

A thin lithium triborate (LBO) crystal of 0.1 mm thickness attached to a thin gold grid was placed on a translation stage to characterize the SHG radiation from the microscope. The SHG signal intensity had a Gaussian distribution along both lateral (horizontal X and vertical Y) directions in the image. The lateral beam spot size on the crystal is 350 µm full width at half maximum (FWHM), and the axial depth of field is 8 µm FWHM with the 20× 0.5 NA objective as determined by the point spread function from 2 µm fluorescing beads.

2.2. Sample preparation

Drosophila melanogaster stocks were grown at 20°C on Bloomington standard cornmeal medium. For static imaging, third instar larvae were dissected along the dorsal midline in calcium-free HL3 saline solution (pH 7.2). Upon removal of internal organs and fat bodies, the body was unfolded to expose the body wall muscles and was fixed in 4% formaldehyde dissolved in 1× phosphate buffered saline (PBS, pH 7.2). The tissue was washed in fresh buffer before preparation for microscopic imaging. The fixed muscles were held between a 1 mm thick microscope slide and a 0.17 mm thick coverslip (No. 1.5), and sealed with nail polish. For live imaging, intact larvae in PBS were squeezed between a microscope slide and a coverslip.

3. Results and discussion

3.1. Wide-field SHG microscopy of fixed larval muscles

We initially explored fixed larval muscles with the 20× 0.5 NA objective lens. A typical SHG image of muscle myofibrils is shown in Fig. 2(a). The image exhibits a periodic structure, originating from the striated pattern of the sarcomere anisotropic bands (A-bands). Due to the large depth of field, the myocytes located at different heights can be visualized in the same image. Optical sectioning with illumination was not employed however, it could help to reduce out of focus background signal. The structure of the myofibrils becomes readily apparent at an incident power above 1.5 W. Optimal imaging was achieved with an incident power of 3.5 W

Biomedical Optics EXPRESS

at the sample providing a signal to noise ratio of 20 dB. Figure 2(b) shows the SHG intensity profile of 15 sarcomeres along a myofibril. The heterogeneity of the intensity of the peaks is attributed to the variation in sarcomere length and structural configuration of myosin nanomotors within myofilaments in the A-bands of sarcomeres. The average sarcomere length is estimated by measuring the M-line-to-M-line distance, which is assumed to be positioned at the peaks in the SHG intensity profile. By applying Gaussian fitting to each peak, the positions of M-lines were determined, yielding an average sarcomere length of 9.1 ± 0.1 μm (mean ± standard error). In order to demonstrate the capability of wide-field SHG microscopy for higher resolution imaging, the 40× 1.3 NA oil objective was also used. Figure 2(c) shows a typical SHG image with a 213 μm × 213 μm field of view. Some myocytes with a double-band structure are visible (circled in Fig. 2(c)). The average sarcomere length is 8.83 ± 0.09 μm in the SHG profile.

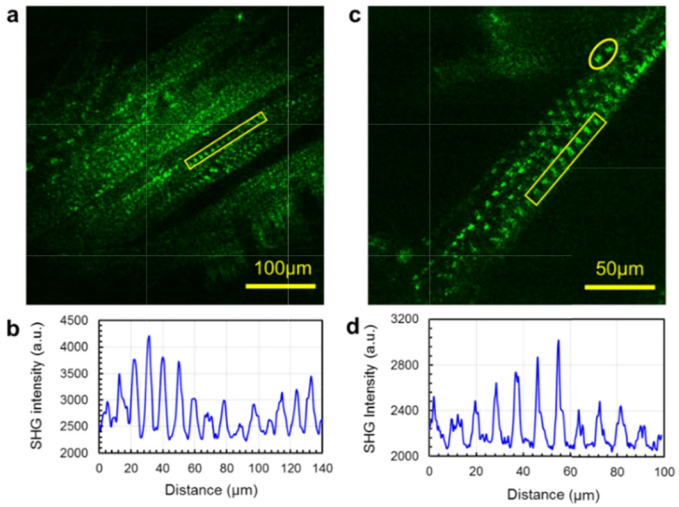

Fig. 2. Fixed larval muscle wide-field SHG images. (a) 425 μm × 425 μm image area (20× 0.5 NA objective), and (c) 213 μm × 213 μm area (40× 1.3 NA oil objective). The laser power at the sample is ~3.0 W and the frame integration time is 100 ms. SHG intensity profiles (b, d) along the myofibrils from the yellow rectangles in (a, c), respectively.

3.2. Wide-field SHG microscopy of contracting larval muscles

Next, we used the wide-field SHG microscope to capture myocyte contractions of live larvae. Figure 3(a) shows the first frame of Visualization 1 that visualizes the active contractions recorded at 10 frames per second for a duration of 30 s, at an incident power of 3 W (2.1 kW/cm^2, 0.035 mJ/cm^2). The viability of myocytes was verified by observing periodic muscle contraction for a duration longer than 1 minute under continuous imaging. With the laser power above 5 W (3.5 kW/cm^2, 0.06 mJ/cm^2) the larva would slow its movement indicating photodamage.

Visualization 1 captures live larva contractions with individual sarcomere length resolution. Live imaging allows the possibility of studying the synchronization of sarcomere shortening and elongation during muscle contraction. Visualization 1 also reveals SHG intensity flickering that is synchronized with changes in sarcomere length. The SHG intensity increase corresponds to the elongation of the sarcomere. The variations of SHG intensity can be monitored live, while measurements of individual sarcomere length require post image processing, hindering live applications. The flickering of sarcomeres was not observed in fixed muscle samples (Fig. 2).

The correlation between sarcomere length and SHG intensity can be studied by analyzing a time series of myofibril segment images over the period of a contraction shown in Fig. 3(b). The

Biomedical Optics EXPRESS

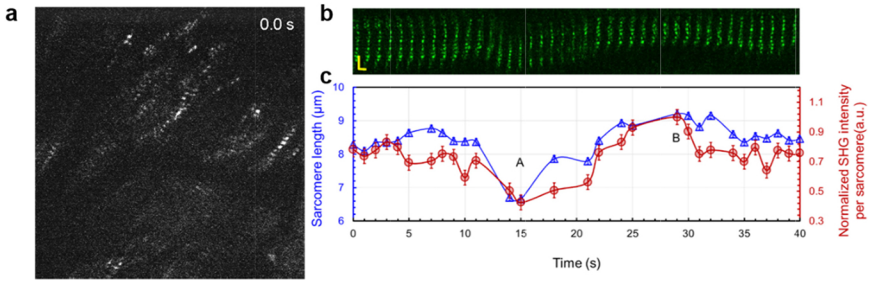

Fig. 3. Dynamics of live larva muscle contraction. (a) The first frame from the wide-field microscope video (425 μm × 425 μm area, 20× 0.5 NA objective, see Visualization 1). (b) Wide-field SHG images of a myofibril over time during a contraction. The horizontal bar shows 0.1 s and the vertical bar is 30 μm. (c) The variation of average sarcomere length (blue triangles) and the normalized SHG intensity per sarcomere (red circles). A few data points are omitted in (c), due to blurring of sarcomeres during fast movement. The A and B labels correspond to shortening and elongation events, respectively.

myofibril segment is selected from Visualization 1. The variation of average sarcomere length and the corresponding variation of SHG intensity are shown in the blue line with triangles and the red line with circles, respectively, in Fig. 3(c). The average sarcomere length is calculated by using an ImageJ (NIH) plugin, SarcOptiM, which uses the fast Fourier transform method [19], and the SHG intensity is averaged for the number of distinguishable sarcomeres (i.e. averaged SHG intensity per sarcomere). During the moment of contraction labeled A in Fig. 3(c), the sarcomeres shorten [20,21] to an average length of 6.7 ± 0.1 μm, and the corresponding average SHG intensity reaches a minimum value. The following moment of relaxation results in stretching of the sarcomeres to an average length of 9.2 ± 0.1 μm (labeled B in Fig. 3(c)) [22,23], and the corresponding SHG intensity increases by more than 50%, indicating a positive correlation between the sarcomere length and the SHG intensity. The correlation of average sarcomere length with SHG intensity matches previous measurements of contracting larva myofibrils imaged with a scanning SHG microscope [5,24].

The linear correlation between sarcomere length and SHG intensity enables live visualization of sarcomere length alterations by monitoring changes in SHG intensity. The SHG intensity changes are easier to monitor compared to the tedious determination of sarcomere length via fitting analysis. A transient intensity decrease corresponds to the sarcomere shortening, while sarcomere elongation results in a transient SHG intensity increase.

4. Conclusion

We have constructed a high-power femtosecond oscillator and wide-field SHG microscope for live imaging of biological specimens. Live muscle contractions were imaged with the wide-field microscope by utilizing the endogenous SHG image contrast originating from the A-bands of sarcomeres. The shortening of larval myocytes is associated with decreasing SHG intensity in individual sarcomeres. Wide-field SHG microscopy of myocytes can be employed as a contractility assay platform for studying arrhythmias and testing cardiac pharmaceutical agents. Wide-field SHG microscopy can also be used for imaging the extracellular matrix collagen in various tissues for cancer diagnostics [4], fibrosis and connective tissue disorders.

Funding

Natural Sciences and Engineering Research Council of Canada (06923, CHRPJ 462842-14); Canadian Institutes of Health Research (CPG-134752).

Biomedical Optics EXPRESS

Disclosures

The authors declare that there are no conflicts of interest related to this article.

References

1. M. E. Llewellyn, R. P. J. Barretto, S. L. Delp, and M. J. Schnitzer, "Minimally invasive high-speed imaging of sarcomere contractile dynamics in mice and humans," Nature **454**(7205), 784–788 (2008).
2. E. Brown, T. McKee, E. DiTomaso, A. Pluen, B. Seed, Y. Boucher, and R. K. Jain, "Dynamic imaging of collagen and its modulation in tumors in vivo using second-harmonic generation," Nat. Med. **9**(6), 796–800 (2003).
3. S. V. Plotnikov, A. C. Millard, P. J. Campagnola, and W. A. Mohler, "Characterization of the myosin-based source for second-harmonic generation from muscle sarcomeres," Biophys. J. **90**(2), 693–703 (2006).
4. A. Golaraei, R. Cisek, S. Krouglov, R. Navab, C. Niu, S. Sakashita, K. Yasufuku, M.-S. Tsao, B. C. Wilson, and V. Barzda, "Characterization of collagen in non-small cell lung carcinoma with second harmonic polarization microscopy," Biomed. Opt. Express **5**(10), 3562–3567 (2014).
5. N. Prent, C. Green, C. Greenhalgh, R. Cisek, A. Major, B. Stewart, and V. Barzda, "Intermyofilament dynamics of myocytes revealed by second harmonic generation microscopy," J. Biomed. Opt. **13**(4), 041318 (2008).
6. C. Macias-Romero, M. E. P. Didier, P. Jourdain, P. Marquet, P. Magistretti, O. B. Tarun, V. Zubkovs, A. Radenovic, and S. Roke, "High throughput second harmonic imaging for label-free biological applications," Opt. Express **22**(25), 31102–31112 (2014).
7. L.-C. Cheng, C.-Y. Chang, C.-Y. Lin, K.-C. Cho, W.-C. Yen, N.-S. Chang, C. Xu, C. Y. Dong, and S.-J. Chen, "Spatiotemporal focusing-based widefield multiphoton microscopy for fast optical sectioning," Opt. Express **20**(8), 8939–8948 (2012).
8. C.-Y. Lin, P.-K. Li, L.-C. Cheng, Y.-C. Li, C.-Y. Chang, A.-S. Chiang, C. Y. Dong, and S.-J. Chen, "High-throughput multiphoton-induced three-dimensional ablation and imaging for biotissues," Biomed. Opt. Express **6**(2), 491–499 (2015).
9. M. Kobayashi, K. Fujita, T. Kaneko, T. Takamatsu, O. Nakamura, and S. Kawata, "Second-harmonic-generation microscope with a microlens array scanner," Opt. Lett. **27**(15), 1324–1326 (2002).
10. C. Macias-Romero, V. Zubkovs, S. Wang, and S. Roke, "Wide-field medium-repetition-rate multiphoton microscopy reduces photodamage of living cells," Biomed. Opt. Express **7**(4), 1458–1467 (2016).
11. R. Le Harzic, I. Riemann, K. König, C. Wüllner, and C. Donitzky, "Influence of femtosecond laser pulse irradiation on the viability of cells at 1035, 517, and 345 nm," J. Appl. Phys. **102**(11), 114701 (2007).
12. K. König, P. T. C. So, W. W. Mantulin, and E. Gratton, "Cellular response to near-infrared femtosecond laser pulses in two-photon microscopes," Opt. Lett. **22**(2), 135–136 (1997).
13. T. Hellerer, A. M. K. Enejder, and A. Zumbusch, "Spectral focusing: High spectral resolution spectroscopy with broad-bandwidth laser pulses," Appl. Phys. Lett. **85**(1), 25–27 (2004).
14. D. Oron, E. Tal, and Y. Silberberg, "Scanningless depth-resolved microscopy," Opt. Express **13**(5), 1468–1476 (2005).
15. E. Tal, D. Oron, and Y. Silberberg, "Improved depth resolution in video-rate line-scanning multiphoton microscopy using temporal focusing," Opt. Lett. **30**(13), 1686–1688 (2005).
16. G. Zhu, J. Van Howe, M. Durst, W. Zipfel, and C. Xu, "Simultaneous spatial and temporal focusing of femtosecond pulses," Opt. Express **13**(6), 2153–2159 (2005).
17. H. Zhao and A. Major, "Powerful 67 fs Kerr-lens mode-locked prismless Yb:KGW oscillator," Opt. Express **21**(26), 31846–31851 (2013).
18. A. Major, V. Barzda, P. A. E. Piunno, S. Musikhin, and U. J. Krull, "An extended cavity diode-pumped femtosecond Yb:KGW laser for applications in optical DNA sensor technology based on fluorescence lifetime measurements," Opt. Express **14**(12), 5285–5294 (2006).
19. C. Pasqualin, F. Gannier, A. Yu, C. O. Malécot, P. Bredeloux, and V. Maupoil, "SarcOptiM for ImageJ: high-frequency online sarcomere length computing on stimulated cardiomyocytes," Am. J. Physiol. Cell Physiol. **311**(2), C277–C283 (2016).
20. D. L. Morgan, D. R. Claflin, and F. J. Julian, "Tension as a function of sarcomere length and velocity of shortening in single skeletal muscle fibres of the frog," J. Physiol. **441**(1), 719–732 (1991).
21. D. E. Rassier, B. R. MacIntosh, and W. Herzog, "Length dependence of active force production in skeletal muscle," J. Appl. Physiol. **86**(5), 1445–1457 (1999).
22. H. L. Granzier and T. C. Irving, "Passive tension in cardiac muscle: contribution of collagen, titin, microtubules, and intermediate filaments," Biophys. J. **68**(3), 1027–1044 (1995).
23. A. Magid and D. J. Law, "Myofibrils bear most of the resting tension in frog skeletal muscle," Science **230**(4731), 1280–1282 (1985).
24. C. Greenhalgh, N. Prent, C. Green, R. Cisek, A. Major, B. Stewart, and V. Barzda, "Influence of semicrystalline order on the second-harmonic generation efficiency in the anisotropic bands of myocytes," Appl. Opt. **46**(10), 1852–1859 (2007).